Science Bulletin 64 (2019) 1875–1880

Contents lists available at ScienceDirect

Science Bulletin

journal homepage: www.elsevier.com/locate/scib

Science Bulletin
www.scibull.com

Article

Cobalt atoms dispersed on hierarchical carbon nitride support as the cathode electrocatalyst for high-performance lithium-polysulfide batteries

Jialing Wu, Junmei Chen, Yang Huang, Kun Feng, Jun Deng, Wei Huang, Yunling Wu, Jun Zhong, Yanguang Li *

Institute of Functional Nano & Soft Materials (FUNSOM), Jiangsu Key Laboratory for Carbon-Based Functional Materials and Devices, Soochow University, Suzhou 215123, China

ARTICLE INFO

Article history:
Received 21 May 2019
Received in revised form 21 July 2019
Accepted 12 August 2019
Available online 14 August 2019

Keywords:
Li-polysulfide battery
Cathode electrocatalyst
Carbon nitride
Cobalt single atom

ABSTRACT

Lithium-sulfur batteries are promising candidates for next-generation energy storage but are confronted with several challenges. One of the possible solutions is to design proper cathode electrocatalysts to accelerate the redox interconversion of solvated polysulfide intermediates. Herein, we report cobalt atoms dispersed on hierarchical carbon nitride support as an effective cathode electrocatalyst for lithium-polysulfide batteries. The electrocatalyst material is prepared from the simple reaction between melamine and cyanuric acid in the presence of Co^{2+}, followed by the Ar annealing. The product has a unique hierarchical structure consisting of many thin and porous C_3N_4 nanosheets finely dispersed with Co atoms. The atomic dispersion of Co species is confirmed by X-ray absorption experiments. Electrochemical measurements reveal that it can promote the interconversion of polysulfides. As a result, batteries using this cathode electrocatalyst achieve large capacity (~1400 mAh/g at 1.6 mA/cm^2), good rate performance (~800 mAh/g at 12.8 mA/cm^2) and impressive cycling stability under different current densities and different sulfur loadings.

1. Introduction

Lithium-ion batteries with high energy density and long lifespan have emerged as the leading choice for energy storage [1]. Unfortunately, they are limited by their relatively high costs and are unable to meet our ever-growing energy demand for future electric vehicles and grid-scale energy storage. It is predicted that the maximum attainable energy density of lithium-ion batteries based on the intercalation chemistry is ~350 Wh/kg [2]. This prompts us to develop alternative technologies beyond lithium-ion batteries. Among many promising candidates, lithium-sulfur batteries clearly stand out by virtue of the earth abundance and low cost of the sulfur cathode as well as the remarkable battery theoretical energy density (2,600 Wh/kg, far exceeding those of current lithium-ion batteries) [3–5]. Despite their great potentials, lithium-sulfur batteries are confronted with several technical hurdles. The most serious one is the soluble polysulfide intermediates escaping from the cathode and shuttling between two electrodes (known as the shuttle effect) [6–9]. This not only leads to the gradual loss of active material and the corrosion of the lithium anode, but also the decrease of overall energy efficiency and battery cycle life.

To address this issue, extensive research efforts have been dedicated to retarding the dissolution of polysulfide intermediates and their escape from the cathode. In early years, many carbonaceous materials were explored as the host materials for their large surface areas and high electrical conductivity to physically constrain polysulfides [10–12]. However, they were generally not very effective due to their nonpolar nature and hence very weak interaction with polysulfides. More recently, polar materials including a variety of metal hydroxides, oxides, nitrides and sulfides are investigated to chemically immobilize polysulfides via stronger polar-polar or Lewis acid-base interactions [9,13–16]. In spite of some encouraging progresses, the dissolution of polysulfide intermediates is still difficult to be effectively suppressed, especially at high sulfur loading such as >4 mg/cm^2. On the other hand, solvated polysulfides are found to play an important role in mediating the charge and discharge process of the sulfur cathode at the electrolyte-electrode interface [17]. If the solvation of polysulfides is completely suppressed, the redox reaction of the sulfur cathode then has to go through a solid-solid phase transition, and its

SPECIAL ISSUE: Emerging Investigators 2019

* Corresponding author.
E-mail address: yanguang@suda.edu.cn (Y. Li).

https://doi.org/10.1016/j.scib.2019.08.016
2095-9273/

reaction kinetics would be significantly slower [15]. This is often observed under the lean electrolyte condition, where the low solubility of short-chain polysulfides results in their considerable precipitation and passivation of the cathode surface, leading to very low sulfur utilization [18]. How to maintain the proper solvation of polysulfides without incurring the shuttle effect holds the decisive key to the future development of high-performance lithium-sulfur batteries.

Recent studies show that the introduction of suitable cathode electrocatalysts to accelerate the redox interconversion of polysulfides may effectively slow down their built-up in the cathode and inhibit their escape from the cathode [15]. This would also permit the pursuit of lithium-polysulfide batteries by directly dissolving polysulfides (Li_2S_6 or Li_2S_8) in the catholyte as the starting active material. Along this line, different electrocatalysts have been developed and investigated for lithium-polysulfide (Li-PS) batteries. For example, Arava and co-workers [19] showed that graphene nanosheets decorated with Pt nanoparticles promoted the polysulfide conversion and achieved higher exchange current density than pure graphene nanosheets. We also demonstrated that W_xC nanoparticles dispersed on the carbonaceous support accelerated the reduction of low-order polysulfides which was otherwise kinetically challenged [20]. Similar catalytic effect was also reported for MoS_2, WS_2, CoS_2, TiN, Co_3S_4 and so on as cathode electrocatalysts [21–31]. Questions remaining are how to further promote their activities while reducing their costs.

In this study, we explore the potential of cobalt atoms dispersed on hierarchical carbon nitride (C_3N_4) support (Co@C_3N_4) as the cathode electrocatalyst to facilitate the redox interconversion of polysulfides in lithium-polysulfide (Li-PS) batteries. C_3N_4 has been widely investigated for photocatalytic and electrocatalytic applications [32,33]. Its intrinsic electrocatalytic activity, however, is far from satisfactory. In this regard, Co atoms are incorporated to the C_3N_4 matrix as the promoter here because they were reported to interact with polysulfides via strong Co-S bonding [31]. Co@C_3N_4 is prepared by annealing the complexes formed from melamine and cyanuric acid in the presence of Co^{2+} ions. Electrochemical measurements reveal that it can promote the interconversion of polysulfides. As a result, batteries using this cathode electrocatalyst achieve large capacity, good rate performance and impressive cycling stability.

2. Experimental

2.1. Preparation of Co@C_3N_4

In a typical synthesis, 15 mL of dimethyl sulfoxide (DMSO) solution containing 0.51 g of cyanuric acid and 0.1 g of cobalt acetate ($Co(OAc)_2{\cdot}4H_2O$) was mixed with 20 mL of DMSO containing 0.50 g of melamine. It immediately gave rise to the solid precipitate (Co-MCA). After further magnetic stirring and ultrasonication for ~20 min, the solid precipitate was collected by centrifugation, repetitively washed with deionized water, and lyophilized. Subsequently, Co-MCA was annealed at 550 °C under Ar for 3 h to yield the final product (Co@C_3N_4). For control experiments, hierarchical C_3N_4 nanostructure was prepared following the same procedure except for the addition of Co precursor at the first step.

2.2. Characterizations

X-ray diffraction (XRD) analysis was carried on a PANalytical X-ray diffractometer with a Cu Kα source at 40 kV. X-ray photoelectron spectroscopy (XPS) measurements were performed on a Thermo Fisher ESCALAB 250Xi X-ray photoelectron spectrometer using Mg as the excitation source. X-ray absorption near edge structure (XANES) and extended X-ray absorption fine structure (EXAFS) measurements were conducted at Beamline 14 W at Shanghai Synchrotron Radiation Facility (SSRF). The product morphology was examined by scanning electron microscopy (SEM, Zeiss Gemini 500) operating at 10.0 kV and transmission electron microscopy (TEM, FEI Tecnai G2 F20) operating at 120.0 kV. Energy dispersive spectroscopy (EDS) elemental mapping was carried out under the scanning transmission electron microscopy (STEM) mode of the TEM.

2.3. Electrochemical measurements

To prepare the cathode, Co@C_3N_4, Super-P carbon black and polyvinylidene fluoride (PVDF) were dispersed in *N*-methyl-2-pyrrolidone (NMP) at the mass ratio of 8:1:1 to form a homogeneous slurry, uniformly coated onto circular carbon cloth current collectors (~1 cm^2), and vacuum-dried at 80 °C for 12 h. The catalyst loading was controlled to be 1 mg/cm^2. Polysulfide-containing catholyte was prepared by dissolving 0.8 g of S_8, 0.23 g of Li_2S, 0.069 g of $LiNO_3$ and 2.87 g of lithium bis(trifluoromethanesulfonyl)imide (LiTFSI) in 10 mL of dioxolane/dimethoxyethane (DOL/DME, 1:1, v:v) under continuously stirring for 24 h. To prepare lithium-polysulfide batteries, the Co@C_3N_4-loaded cathode was impregnated with a calculated volume of the catholyte (21 μL for 2 mg/cm^2 of equivalent sulfur normalized to the cathode area, or 42 μL for 4 mg/cm^2 of equivalent sulfur). It was further paired with a Li disk anode and a Celgard 2340 polypropylene membrane separator, and added with 30 μL of blank electrolyte (1 mol/L LiTFSI and 0.5 mol/L $LiNO_3$ in DOL/DME) to the anode side in standard CR2032 coin cells. Lithium-polysulfide batteries were tested for cyclic voltammogram (CV) between 1.7 and 2.8 V at a scan rate of 0.05 mV/s on a CHI660E potentiostat, or in the galvanostatic mode within the same voltage window on a NEWARE multichannel battery tester.

3. Results and discussion

3.1. Structural characterizations of Co-MCA and Co@C_3N_4

We prepared Co@C_3N_4 via a two-step process as schematically illustrated in Fig. 1a. At the first step, melamine (MA) was reacted with cyanuric acid (CA) together with Co^{2+} ions in the DMSO solution (Fig. 1a). This gave rise to a solid precipitate composed of two-dimensional MA/CA network interconnected via multiple hydrogen bonds and dispersed with Co^{2+}. The solid precipitate is named as Co-MCA for short. When examined under SEM, Co-MCA is revealed to have a flower-like hierarchical structure with a diameter of 1–2 μm (Fig. 1b). Each flower further consists of well-organized nanoflakes having a lateral size of 100–200 nm and protruding from the center (Fig. 1c). For the second step, Co-MCA was annealed in Ar at 550 °C for 3 h. During the annealing, the MA/CA network was converted to C_3N_4 with the tri-s-triazine structure. Co atoms were believed to remain immobilized on the support. The final product is named as Co@C_3N_4. It has a dark-yellow color instead of the light-yellow color characteristic to C_3N_4, signaling the incorporation of Co atoms (inset of Fig. 1d). Co@C_3N_4 is observed to resemble microsized doughnuts with hollow centers from SEM (Fig. 1c and d). The original nanoflakes are transformed to curvy nanosheets with significantly reduced thickness and abundant porosity due to the structural condensation and partial sublimation of C_3N_4. Under TEM, the porosity of Co@C_3N_4 becomes more evident (Fig. 1f and g). It renders Co@C_3N_4 with large surface areas ideal for electrocatalytic applications. BET analysis of Co@C_3N_4 suggests that it has a surface area of 89.5 m^2/g and pore volume of 0.08 m^3/g (Fig. S1 online). In our best knowledge, such a hierarchical and porous structure is unique and not

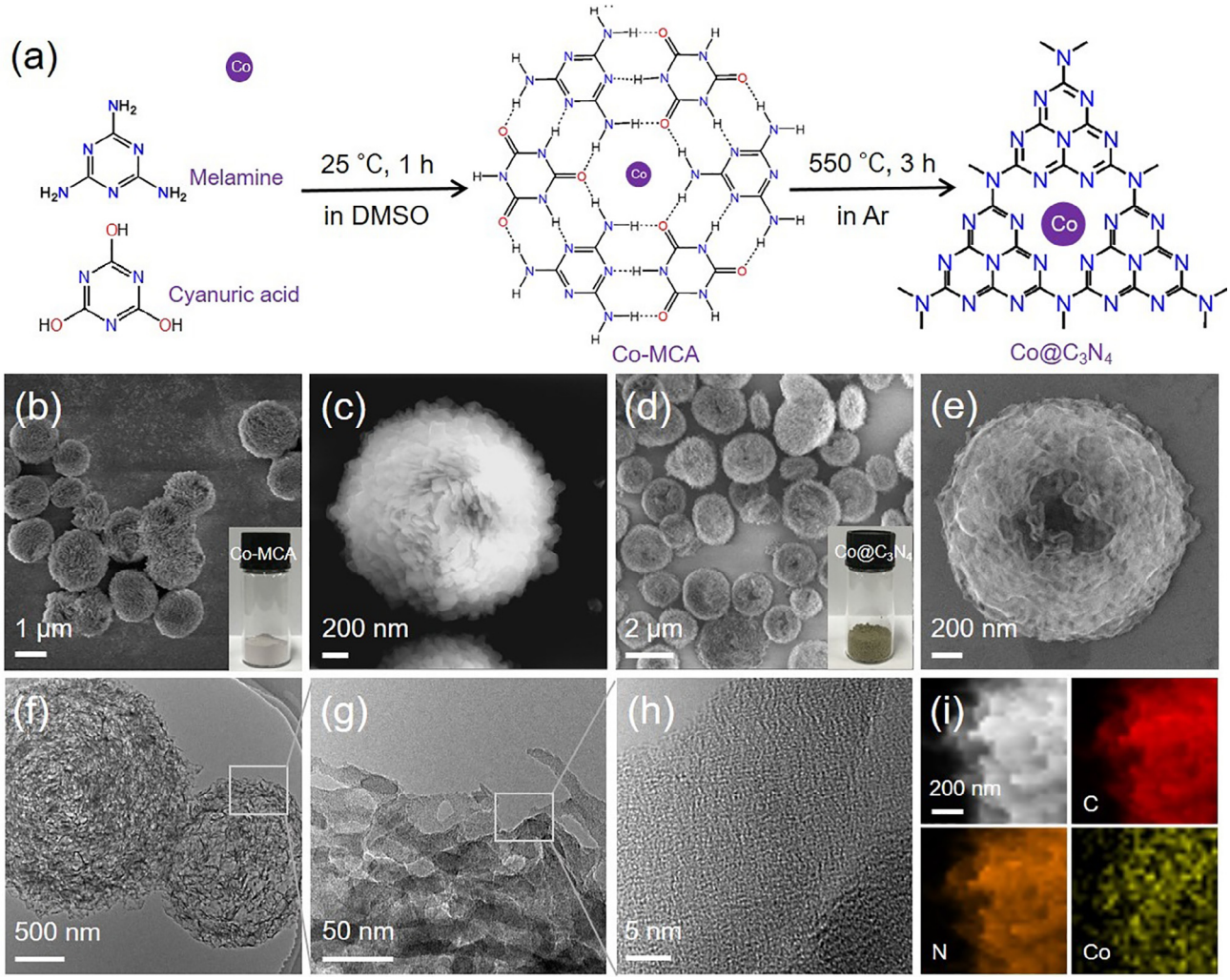

Fig. 1. (Color online) (a) Schematic synthetic procedure for Co@C_3N_4. (b, c) SEM images of Co-MCA at low and high magnifications. (d, e) SEM images of Co@C_3N_4 at low and high magnifications. (f–h) TEM images of Co@C_3N_4. (i) Corresponding C, N and Co EDS elemental mapping of Co@C_3N_4.

readily attainable from the conventional thermal condensation of melamine or urea [34]. High-resolution TEM image reveals that the C_3N_4 support is largely amorphous (Fig. 1h). No free or supported Co or CoO_x clusters or nanoparticles are observed over a large scale, indicating that Co species are finely dispersed. Moreover, EDS elemental mapping of C, N and Co was carried out under STEM, and its results are depicted in Fig. 1i. The spatial distribution of Co species is roughly in agreement with that of C or N, which evidences that Co is uniformly dispersed over the entire C_3N_4 support. For control experiments, Co-free C_3N_4 was also prepared under the same conditions except for the addition of Co precursor. The resultant final product presents a similar morphology to Co@C_3N_4 (Fig. S2 online). It is also measured to have a similar surface area and pore volume as Co@C_3N_4 (Fig. S1 online).

Co@C_3N_4 was further interrogated by several spectroscopic techniques. XRD pattern of Co@C_3N_4 shows two peaks at 13.2° and 27.4° assignable to the (1 0 0) and (0 0 2) diffractions of layered C_3N_4 (Fig. 2a). The lack of Co or CoO_x signals again corroborates the fine dispersion of Co atoms on the C_3N_4 support. XPS analysis of the final product at the C 1s region features two pronounced peaks from C–C bonds (at 284.7 eV) and C=N–C bonds (at 288.1 eV) characteristic to C_3N_4 (Fig. 2b) [34]. The N 1s XPS spectrum shows a big envelope, and its deconvolution unveils the contributions from C=N–C (at 398.7 eV), N–C_3 (at 399.8 eV) and C–N–H (at 401.2 eV) (Fig. 2c). This result is also in line with previous observations with C_3N_4 [35]. Importantly, Co 2p XPS of Co@C_3N_4 displays two discernible but low intensity peaks, supporting the presence but low concentration of Co dispersed on the C_3N_4 support (Fig. 2d). The binding energy of the Co $2p_{3/2}$ peak most closely matches those of divalent or trivalent Co compounds instead of metallic Co. It is worth noting that previous studies about transition metals supported on C_3N_4 suggested that they were most likely in their ionic states and presumably stabilized via their interactions with N atoms [34,36]. Furthermore, we conducted XANES and EXAFS analysis of Co@C_3N_4. The absorption edge of Co K-edge XANES is close to but slightly more positive than that of CoO, evidencing that Co in Co@C_3N_4 is between bivalent and trivalent (Fig. 2e). Corresponding Fourier transform EXAFS of Co@C_3N_4 exhibits pronounced Co–O bonding signal at ~1.5 Å but is devoid of Co–Co bonding signal at ~2.5 Å (Fig. 2f). This indicates that Co species in the final product is atomically dispersed.

3.2. Electrochemical performance of Co@C_3N_4 as the cathode electrocatalyst

To investigate the potential of Co@C_3N_4 as the cathode electrocatalyst for lithium-polysulfide (Li-PS) batteries, it was blended with carbon black additive and PVDF binder, and drop-cast onto

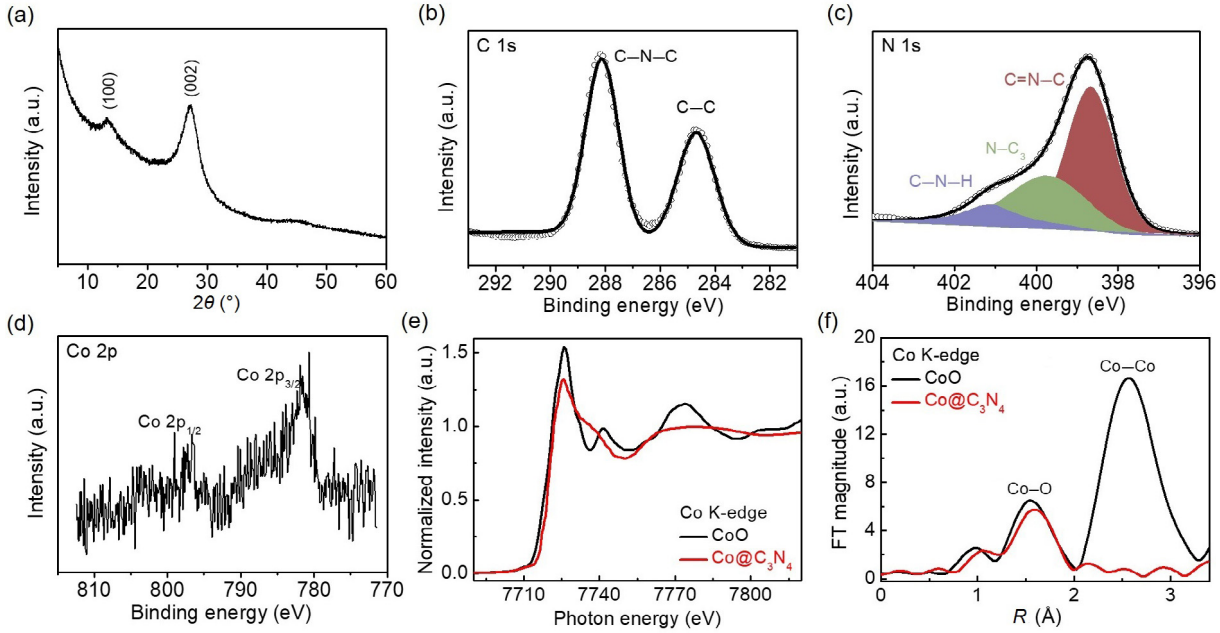

Fig. 2. (Color online) (a) XRD pattern of $Co@C_3N_4$. (b) C 1s XPS, (c) N 1s XPS and (d) Co 2p XPS of $Co@C_3N_4$. (e) Co K-edge XANES and (f) corresponding EXAFS of $Co@C_3N_4$ in comparison with the CoO reference.

a circular carbon cloth current collector to reach a catalyst loading of ~1 mg/cm^2. Polysulfide-containing catholyte was prepared by reacting stoichiometric amounts of Li_2S and S_8 in the electrolyte solution. The $Co@C_3N_4$-loaded cathode was then impregnated with a calculated amount of catholyte to achieve an equivalent sulfur loading of 2–4 mg/cm^2 (normalized over the cathode area) in standard coin cells.

First of all, we assessed the reaction process of our Li-PS battery with $Co@C_3N_4$ via CV at 0.05 mV/s (Fig. 3a). It exhibits two cathodic peaks centered at 2.29 and 2.0 V. The former is typically assigned to the reduction from Li_2S_6/Li_2S_8 to Li_2S_4, whereas the latter is assignable to the further reduction of Li_2S_4 to Li_2S_2/Li_2S [37]. When the sweeping direction is reversed, the CV curve exhibits an envelope of anodic peaks at 2.4–2.5 V that corresponds to the re-oxidation of Li_2S_2/Li_2S to Li_2S_6/Li_2S_8. Consistent results are also obtained from the galvanostatic charge-discharge measurement with the equivalent sulfur loading of 2 mg/cm^2 and at 1.6 mA/cm^2 (corresponding to 0.5 C). As shown in Fig. 3b, the discharge curve shows two distinct plateaus at ~2.3 and ~2.0 V, and its charge curve has a long and gradually increasing plateau between 2.3 and 2.5 V. The initial discharge capacity reaches ~1,400 mAh/g, and ~1,350 mAh/g is recovered upon the recharge.

To investigate the cycling performance, our Li-PS battery containing 2 mg/cm^2 of sulfur was cycled at 1.6 mA/cm^2. Its specific

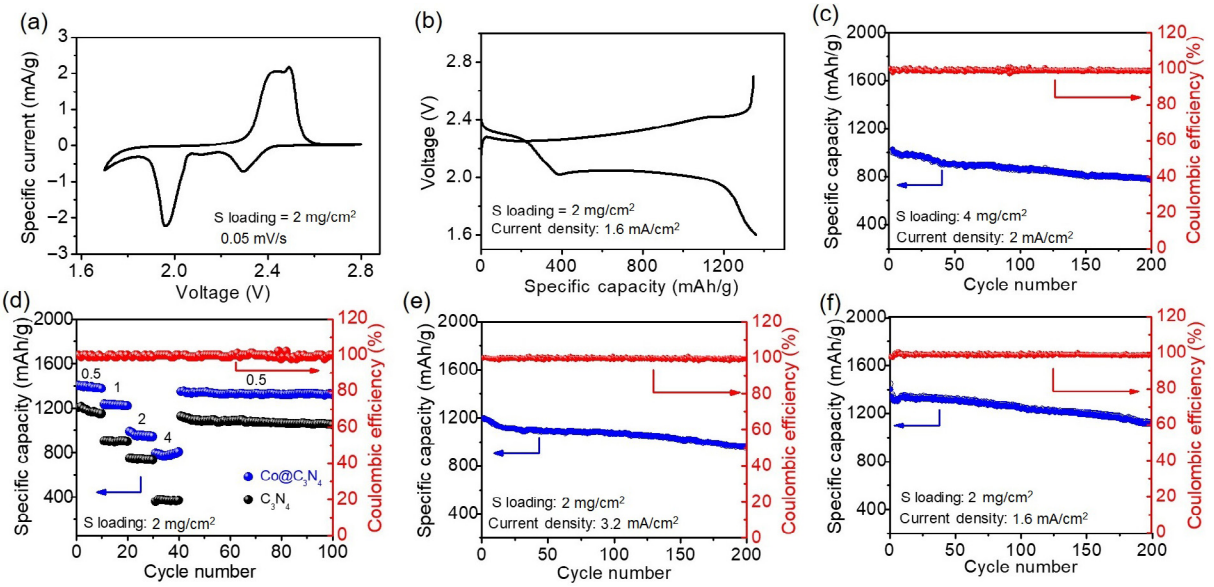

Fig. 3. (Color online) (a) CV curves of $Co@C_3N_4$ as the cathode electrocatalyst. (b) Galvanostatic charge and discharge curves of $Co@C_3N_4$ as the cathode electrocatalyst. (c) Cycling stability of the Li-PS battery using $Co@C_3N_4$ as the cathode electrocatalyst at 1.6 mA/cm^2. (d) Rate capability of Li-PS batteries using C_3N_4 or $Co@C_3N_4$ as the cathode electrocatalyst. (e) Cycling stability of the Li-PS battery using $Co@C_3N_4$ as the cathode electrocatalyst at 3.2 mA/cm^2. (f) Cycling stability of the Li-S battery using $Co@C_3N_4$ as the cathode electrocatalyst with 4 mg/cm^2 of equivalent sulfur at 2 mA/cm^2.

capacity is observed to slowly decrease from the original ~1,400 mAh/g to ~1,160 mAh/g at the end of 200 cycles (Fig. 3c). This translates to an impressively small capacity loss of 0.09% per cycle. The corresponding Coulombic efficiency is found to stay close to unity after the first few cycles. When the current rate is raised from 1.6 to 3.2, 6.4 and 12.8 mA/cm^2, the battery retains considerable discharge capacity of 1,226, 953 and 782 mAh/g, respectively (Fig. 3d). When the current rate is reverted back to 1.6 mA/cm^2, ~1,330 mAh/g is recovered. These results underline the great rate capability of our Li-PS batteries with Co@C_3N_4 as the cathode electrocatalyst. By stark contrast, replacing Co@C_3N_4 with metal-free C_3N_4 results in inferior electrochemical performance, especially under large currents. For example, Li-PS battery with C_3N_4 as the cathode electrocatalyst exhibits discharge capacity of ~370 mA/cm^2 at 12.8 mA/cm^2 — only half that of Co@C_3N_4. It therefore highlights the important role of Co atoms in expediting the redox interconversion of polysulfide intermediates. Furthermore, higher current density does not compromise the cycling stability. The Li-PS battery with Co@C_3N_4 retains ~980 mAh/g at the end of 200 cycles when cycled at 3.2 mA/cm^2 (1 C) (Fig. 3e). We also demonstrate that our batteries are capable of reversibly functioning under higher sulfur loading. Fig. 3f shows the cycling stability with 4 mg/cm^2 of sulfur at 2 mA/cm^2. Remarkable capacity of ~780 mAh/g is still retained after 200 cycles. The combination of large specific capacity, great rate capability, the possibility to work under large current density or large sulfur loading renders our batteries highly competitive among reported studies. This would be impossible if it was not for excellent electrocatalytic activity of Co@C_3N_4 [38–40].

4. Conclusion

In summary, we demonstrated Co@C_3N_4 as a promising cathode electrocatalyst for Li-PS batteries. It was prepared from the reaction between melamine and cyanuric acid in the presence of Co^{2+}, followed by Ar annealing. The resultant product had a hierarchical structure consisting of many thin and porous nanosheets. Microscopic and spectroscopic characterizations confirmed the fine dispersion of Co atoms over the high-surface-area C_3N_4 support. When used as the cathode electrocatalyst in Li-PS batteries, Co@C_3N_4 enabled large specific capacity (~1,400 mAh/g at 1.6 mA/cm^2), great rate capacity (~800 mAh/g at 12.8 mA/cm^2), and impressive cycling stability under different current densities and different sulfur loadings. Our study here provides a new strategy toward the rational design and preparation of transition metal loaded C_3N_4 materials, and unveils their great potentials for future lithium-sulfur or lithium-polysulfide batteries.

Conflict of interest

The authors declare that they have no conflict of interest.

Acknowledgments

This work was supported by the Priority Academic Program Development of Jiangsu Higher Education Institutions and Collaborative Innovation Center of Suzhou Nano Science and Technology.

Author contributions

Yanguang Li conceived the project and designed the experiment. Jialing Wu and Junmei Chen prepared the material and performed battery measurements. Kun Feng and Jun Zhong carried out XANES and EXAFS analysis. Jun Deng performed TEM imaging and EDS mapping. Yang Huang and Wei Huang assisted in data analysis. Jialing Wu and Yanguang Li co-wrote the manuscript.

Appendix A. Supplementary data

Supplementary data to this article can be found online at https://doi.org/10.1016/j.scib.2019.08.016.

References

[1] Li M, Lu J, Chen ZW, et al. 30 years of lithium-ion batteries. Adv Mater 2018;30:1800561.
[2] Manthiram A. An outlook on lithium ion battery technology. ACS Central Sci 2017;3:1063–9.
[3] Pang Q, Liang X, Kwok CY, et al. Advances in lithium-sulfur batteries based on multifunctional cathodes and electrolytes. Nat Energy 2016;1:16132.
[4] Manthiram A, Fu YZ, Chung SH, et al. Rechargeable lithium-sulfur batteries. Chem Rev 2014;114:11751–87.
[5] Seh ZW, Sun YM, Zhang QF, et al. Designing high-energy lithium-sulfur batteries. Chem Soc Rev 2016;45:5605–34.
[6] Fang RP, Zhao SY, Sun ZH, et al. More reliable lithium-sulfur batteries: status, solutions and prospects. Adv Mater 2017;29:1606823.
[7] Yang Y, Zheng GY, Cui Y. Nanostructured sulfur cathodes. Chem Soc Rev 2013;42:3018–32.
[8] Song MK, Cairns EJ, Zhang YG. Lithium/sulfur batteries with high specific energy: old challenges and new opportunities. Nanoscale 2013;5:2186–204.
[9] Liu X, Huang JQ, Zhang Q, et al. Nanostructured metal oxides and sulfides for lithium-sulfur batteries. Adv Mater 2017;29:1601759.
[10] Ji XL, Lee KT, Nazar LF. A highly ordered nanostructured carbon-sulphur cathode for lithium-sulphur batteries. Nat Mater 2009;8:500–6.
[11] Liang J, Sun ZH, Li F, et al. Carbon materials for Li-S batteries: functional evolution and performance improvement. Energy Storage Mater 2016;2:76–106.
[12] Xu ZL, Kim JK, Kang K. Carbon nanomaterials for advanced lithium sulfur batteries. Nano Today 2018;19:84–107.
[13] Manthiram A, Chung SH, Zu CX. Lithium-sulfur batteries: progress and prospects. Adv Mater 2015;27:1980–2006.
[14] Peng HJ, Huang JQ, Cheng XB, et al. Review on high-loading and high-energy lithium-sulfur batteries. Adv Energy Mater 2017;7:1700260.
[15] Liu DH, Zhang C, Zhou GM, et al. Catalytic effects in lithium-sulfur batteries: promoted sulfur transformation and reduced shuttle effect. Adv Sci 2018;5:1700270.
[16] Li Z, Ma ZL, Wang YY, et al. LDHs derived nanoparticle-stacked metal nitride as interlayer for long-life lithium sulfur batteries. Sci Bull 2018;63:169–75.
[17] Fan FY, Chiang YM. Electrodeposition kinetics in Li-S batteries: effects of low electrolyte/sulfur ratios and deposition surface composition. J Electrochem Soc 2017;164:A917–22.
[18] Zhang G, Peng HJ, Zhao CZ, et al. The radical pathway based on a lithium-metal-compatible high-dielectric electrolyte for lithium-sulfur batteries. Angew Chem Int Ed 2018;57:16732–6.
[19] Al Salem H, Babu G, Rao CV, et al. Electrocatalytic polysulfide traps for controlling redox shuttle process of Li-S batteries. J Am Chem Soc 2015;137:11542–5.
[20] Wu YL, Zhu XR, Li PR, et al. Ultradispersed W_xC nanoparticles enable fast polysulfide interconversion for high-performance Li-S batteries. Nano Energy 2019;59:636–43.
[21] Wang HT, Zhang QF, Yao HB, et al. High electrochemical selectivity of edge versus terrace sites in two-dimensional layered MoS_2 materials. Nano Lett 2014;14:7138–44.
[22] Babu G, Masurkar N, Al Salem H, et al. Transition metal dichalcogenide atomic layers for lithium polysulfides electrocatalysis. J Am Chem Soc 2016;139:171–8.
[23] Zhou GM, Tian HZ, Jin Y, et al. Catalytic oxidation of Li_2S on the surface of metal sulfides for Li-S batteries. Proc Natl Acad Sci USA 2017;114:840–5.
[24] Jeong TG, Choi DS, Song H, et al. Heterogeneous catalysis for lithium-sulfur batteries: enhanced rate performance by promoting polysulfide fragmentations. ACS Energy Lett 2017;2:327–33.
[25] Pu J, Shen ZH, Zheng JX, et al. Multifunctional Co_3S_4@sulfur nanotubes for enhanced lithium-sulfur battery performance. Nano Energy 2017;37:7–14.
[26] Tao X, Wang J, Liu C, et al. Balancing surface adsorption and diffusion of lithium-polysulfides on nonconductive oxides for lithium-sulfur battery design. Nat Commun 2016;7:11203.
[27] Yuan HD, Chen XL, Zhou GM, et al. Efficient activation of Li_2S by transition metal phosphides nanoparticles for highly stable lithium-sulfur batteries. ACS Energy Lett 2017;2:1711–9.
[28] Mi YY, Liu W, Li XL, et al. High-performance Li-S battery cathode with catalyst-like carbon nanotube-MoP promoting polysulfide redox. Nano Res 2017;10:3698–705.
[29] Yang YX, Zhong YR, Shi QW, et al. Electrocatalysis in lithium sulfur batteries under lean electrolyte conditions. Angew Chem Int Ed 2018;57:15549–52.
[30] Yuan HD, Zhang WK, Wang JG, et al. Facilitation of sulfur evolution reaction by pyridinic nitrogen doped carbon nanoflakes for highly-stable lithium-sulfur batteries. Energy Storage Mater 2018;10:1–9.

[31] Zhong YR, Yin LC, He P, et al. Surface chemistry in cobalt phosphide-stabilized lithium-sulfur batteries. J Am Chem Soc 2018;140:1455–9.
[32] Xu Y, Kraft M, Xu R. Metal-free carbonaceous electrocatalysts and photocatalysts for water splitting. Chem Soc Rev 2016;45:3039–52.
[33] Huang W, He Q, Hu YP, et al. Molecular heterostructures of covalent triazine frameworks for highly enhanced photocatalytic hydrogen production. Angew Chem Int Ed 2019;58:8676–80.
[34] Ong WJ, Tan LL, Ng YH, et al. Graphitic carbon nitride (g-C_3N_4)-based photocatalysts for artificial photosynthesis and environmental remediation: are we a step closer to achieving sustainability? Chem Rev 2016;116:7159–329.
[35] Lakhi KS, Park DH, Al-Bahily K, et al. Mesoporous carbon nitrides: synthesis, functionalization, and applications. Chem Soc Rev 2017;46:72–101.
[36] Du ZZ, Chen XJ, Hu W, et al. Cobalt in nitrogen-doped graphene as single-atom catalyst for high-sulfur content lithium-sulfur batteries. J Am Chem Soc 2019;141:3977–85.
[37] Xu R, Lu J, Amine K. Progress in mechanistic understanding and characterization techniques of Li-S batteries. Adv Energy Mater 2015;5:1500408.
[38] Pang Q, Liang X, Kwok CY, et al. A comprehensive approach toward stable lithium-sulfur batteries with high volumetric energy density. Adv Energy Mater 2017;7:1601630.
[39] Yang Y, Zheng GY, Cui Y. A membrane-free lithium/polysulfide semi-liquid battery for large-scale energy storage. Energy Environ Sci 2013;6:1552–8.
[40] Fu YZ, Su YS, Manthiram A. Highly reversible lithium/dissolved polysulfide batteries with carbon nanotube electrodes. Angew Chem Int Ed 2013;52:6930–5.

Jialing Wu received her B.S. degree in College of Energy from Soochow University in 2018. She currently is a Master student under the supervision of Prof. Yanguang Li at FUNSOM of Soochow University. Her current research interests focus on lithium-sulfur battery, sodium-ion batteries and potassium-ion batteries.

Yanguang Li is a Professor at FUNSOM of Soochow University, China. He received his Ph.D. degree in Chemistry from Ohio State University in 2010, and then moved to Stanford University and completed a post-doctoral training before taking the current faculty position in 2013. His research focuses on nanostructured functional materials for energy applications, particularly in the realm of advanced batteries and electrocatalysis.